Developmental differences in canonical cortical networks: insights from microstructure-informed tractography

Sila Genc[1,2,3*], Simona Schiavi[1,4,5*], Maxime Chamberland[1,6], Chantal M.W. Tax[7,8], Erika P. Raven[1,9], Alessandro Daducci[4], Derek K. Jones[1]

[1] Cardiff University Brain Research Imaging Centre (CUBRIC), School of Psychology, Cardiff University, Cardiff, United Kingdom
[2] Neuroscience Advanced Clinical Imaging Service (NACIS), Department of Neurosurgery, The Royal Children's Hospital, Parkville, Victoria, Australia
[3] Developmental Imaging, Clinical Sciences, Murdoch Children's Research Institute, Parkville, Victoria, Australia
[4] Department of Computer Science, University of Verona, Italy
[5] ASG Superconductors S.p.A., Genova, Italy
[6] Eindhoven University of Technology, Department of Mathematics and Computer Science, Eindhoven, The Netherlands
[7] Image Sciences Institute, University Medical Center Utrecht, Utrecht, The Netherlands
[8] Cardiff University Brain Research Imaging Centre (CUBRIC), School of Physics and Astronomy, Cardiff University, UK
[9] Center for Biomedical Imaging, Department of Radiology, New York University Grossman School of Medicine, New York, USA

*authors contributed equally

Corresponding Author
Sila Genc
Department of Neurosurgery
Royal Children's Hospital
Parkville, Victoria, Australia
E: sila.genc@mcri.edu.au

Short title: Developmental differences in microstructure-informed brain networks

Keywords
Development, connectivity, microstructure informed tractography, cortical, diffusion

Abstract

In response to a growing interest in refining brain connectivity assessments, this study focuses on integrating white matter fibre-specific microstructural properties into structural connectomes. Spanning ages 8-19 years in a developmental sample, it explores age-related patterns of microstructure-informed network properties at both local and global scales.

First the diffusion-weighted signal fraction associated with each tractography-reconstructed streamline was constructed. Subsequently, the Convex Optimization Modelling for Microstructure-Informed Tractography (COMMIT) approach was employed to generate microstructure-informed connectomes from diffusion MRI data. To complete the investigation, network characteristics within eight functionally defined networks (visual, somatomotor, dorsal attention, ventral attention, limbic, frontoparietal, default mode, and subcortical networks) were evaluated.

The findings underscore a consistent increase in global efficiency across child and adolescent development within the visual, somatomotor, and default mode networks ($p<.005$). Additionally, mean strength exhibits an upward trend in the somatomotor and visual networks ($p<.001$). Notably, nodes within the dorsal and ventral visual pathways manifest substantial age-dependent changes in local efficiency, aligning with existing evidence of extended maturation in these pathways. The outcomes strongly support the notion of a prolonged developmental trajectory for visual association cortices.

This study contributes valuable insights into the nuanced dynamics of microstructure-informed brain connectivity throughout different developmental stages.

1. Introduction

The transition from childhood to adolescence is a period of profound neurobiological and cognitive development where the human brain undergoes significant changes to refine neural substrates prior to adulthood (Blakemore & Choudhury, 2006). Essential to this process are the white matter pathways that form a structural scaffold facilitating connections and communication between cortical regions. Their development follows a stereotypical pattern of myelination, which closely mirrors the functional capacity of neural systems. For example, primary sensory, motor and visual pathways typically complete myelination by the first two years of life (Deoni et al., 2015), whereas frontal and temporal association regions continue to develop well into adulthood, with peak myelination happening in the second decade of life (Bartzokis et al., 2012; Yakovlev & Lecours, 1967). The process of axonal development is less clear, with early *ex vivo* studies indicating stabilization of corpus callosum axonal count by six months of age (LaMantia & Rakic, 1990) and further work indicating changes to axonal and myelin properties at pubertal onset (Genc et al., 2023; Juraska & Willing, 2017; Paus, 2010).

Developmental studies using magnetic resonance imaging (MRI) have revealed that white matter volume steadily increases over childhood and adolescence (Giedd et al., 1999; Lenroot & Giedd, 2006), likely by way of coupled radial growth of the axon and myelin sheath. In tandem, functional MRI (fMRI) studies suggest a greater degree of temporal network connectivity, which remodels from infancy to early adulthood (Grayson & Fair, 2017). Early in childhood, sensorimotor systems become well integrated and coordinated, and show little change into adulthood (Gu et al., 2015). Later in adolescence, functional hubs such as fronto-parietal, attentional and salience networks become increasingly segregated, allowing for flexibility as the adolescent brain becomes more adaptable to increase performance and efficiency (Danielle S Bassett et al., 2011).

Diffusion magnetic resonance imaging (dMRI) has enabled novel discoveries in spatial and temporal patterns of white matter fibre development (Geeraert et al., 2019; Genc et al., 2018; Herting et al., 2017; Lebel & Beaulieu, 2011; Palmer et al., 2022; Tamnes et al., 2018). Structural connectivity has been studied using diffusion MRI tractography (Hagmann et al., 2007) to reconstruct white matter pathways or connections between nodes of interest (e.g., between

distinct predefined cortical regions). Connection strength is commonly defined using streamline count, i.e., the number of streamlines, derived from tractography, that run between nodes. However, this notion can be arbitrary, since streamline count is not biologically informative and can heavily depend on acquisition and processing parameters (D. K. Jones et al., 2013; Yeh et al., 2021; Zhang et al., 2022). Recent studies have attempted to improve the *status quo* in determining biologically informative determinants of connection strength using diffusion MRI (Smith et al., 2020; Zhang et al., 2022), however, the question remains: which measures are optimally informative?

To define more informative edge weights for the structural connectome, the 'tractometry' approach was introduced in (Bells et al., 2011; Jones et al., 2006; Kanaan et al., 2006) and employed to study typical white matter development (Chamberland et al., 2019). This approach includes the mapping of microstructural measures along tractography-reconstructed pathways and computing average values for quantitative comparisons between measures. A challenge arises when multiple bundles pass through the same imaging voxel (an extremely prevalent phenomena; see Jeurissen et al. (2013); Schilling et al. (2022)) leading to biased measures assigned to each constituent bundle (Schiavi et al., 2022). The Convex Optimization Modelling for Microstructure Informed Tractography (COMMIT) (Daducci et al., 2015; Daducci et al., 2013) approach address this problem by deconvolving specific microstructural features on each streamline to recover individual contributions to the measured signal. By replacing the commonly used streamline count with intra-axonal signal fraction (IASF), it offers a quantitative and more biologically informative assessment of brain connectivity (Bergamino et al., 2022; Gabusi et al., 2022; Schiavi et al., 2022; Schiavi, Ocampo-Pineda, et al., 2020; Schiavi, Petracca, et al., 2020).

To investigate age-related differences in structural connectivity among various canonical or domain-specific networks, graph theory provides a powerful analytical tool (Fornito et al., 2016; Zhang et al., 2022). Graph theoretical analysis permits the computation of networks at different levels of organization (Fornito et al., 2016; Yeh et al., 2021), using measures classified as (i) local (quantifying properties of individual nodes), (ii) mesoscale (describing interconnected clusters of nodes); and (iii) global (describing whole-brain connectivity properties) (Fornito et al., 2016; Rubinov & Sporns, 2010). At the global scale, graph measures reveal how the brain's structural wiring facilitates

information communication between distant regions and cognitive systems. While structurally connected regions can communicate directly, signal propagation between unconnected nodes requires a sequence of one or more intermediate connections (Zhang et al., 2022). Thus, investigating these measures across and between predefined cognitive systems during development can shed light on the structural mechanisms behind functional expression (Seguin et al., 2019).

Given it has been shown that white matter microstructure, at the voxel and tract level, continues to develop well into the third decade of life (Lebel & Beaulieu, 2011; Lebel & Deoni, 2018), we were interested in studying how *network* properties mature from childhood to adolescence when weighted by their microstructural properties. Here we construct microstructure-informed connectomes and study age-related patterns of commonly-used local and global structural brain network properties in a typically developing sample aged 8-19 years.

2. Materials and methods

2.1. Participants

We enrolled a sample of typically developing children and adolescents aged 8-19 years recruited as part of the Cardiff University Brain Research Imaging Centre (CUBRIC) Kids study, with ethical approval from the School of Psychology ethics committee at Cardiff University. Participants and their parents/guardians were recruited via public outreach events, and written informed consent was obtained from the primary caregiver of each child participating in the study. Adolescents aged 16-19 years additionally provided written consent. Children were excluded from the study if they had non-removable metal implants, or a reported history of a major head injury or epilepsy. All procedures were conducted in accordance with the Declaration of Helsinki. A total of 88 children (Mean age = 12.6, SD = 2.9 years) were included in the current study (46 female).

2.2. MRI acquisition

Images were acquired on a 3T Siemens Connectom system with ultra-strong (300 mT/m) gradients. As described in (Genc et al., 2020), the protocol comprised: (a) a 3D Magnetization Prepared Rapid Gradient Echo (MPRAGE) for structural segmentation (TE/TR = 2/2300ms; voxel size $1\times1\times1mm^3$); (b) multi-shell dMRI acquisition (TE/TR = 59/3000 ms; voxel size = $2\times2\times2mm^3$) with $b\in$[500, 1200, 2400, 4000, 6000] s/mm^2 in 30, 30, 60, 60, 60 directions respectively and additional 14 b = 0 s/mm^2 volumes. Diffusion MRI data were acquired in an anterior-posterior phase-encoding direction, with one additional posterior-anterior volume.

2.3. MRI processing

A summary of image processing steps is illustrated in Figure 1. T_1-weighted data were processed using FreeSurfer version 6.0 (http://surfer.nmr.mgh.harvard.edu) to derive a white matter mask and parcellate the cortical grey matter according to the Destrieux atlas (Destrieux et al., 2010). Next, we registered the Yeo functional atlas (Yeo et al., 2011) in MNI space to each individual subject's space using a non-linear transformation as implemented in FNIRT of FSL (Smith et al., 2004). This allowed us to obtain eight functionally relevant cortical canonical networks (herein referred to as "Yeo7") for further interrogation (visual, somatomotor, dorsal attention, ventral attention, limbic, frontoparietal, default mode network, subcortical). Subsequently, we grouped regions of interest (ROIs) from the Destrieux atlas into the eight Yeo atlas networks. To merge the two atlases within each subject, we employed a data-driven approach (see Baum et al. (2017)). Briefly, each parcellated brain region was assigned to one of eight canonical functional brain networks (Yeo et al., 2011) by considering the maximum number of voxels in the intersection between the masks. We ensured that the same overlap was confirmed in the homologous ROIs and for at least 80% of the enrolled subjects, discarding any Destrieux ROIs that did not meet these criteria. The final subdivision can be seen in Figure 2 and Table S2. Finally, we linearly-registered the T_1-weighted images and the corresponding parcellations on dMRI data using FLIRT (Jenkinson et al., 2002) with boundary-based optimization (Greve & Fischl, 2009). To investigate whether any result was robust against atlas choice, we repeated the same process with cortical parcellation using the Desikan-Killany atlas (Desikan et al., 2006) and by grouping nodes into five distinct lobes (frontal, parietal, temporal, occipital, subcortical).

Diffusion MRI data were pre-processed as detailed in Genc et al. (2020). Briefly the preprocessing pipeline involved FSL (Smith et al., 2004), MRtrix3 (Tournier et al., 2019), and ANTs (Avants et al., 2011) tools using the following steps: denoising (Veraart et al., 2016); slice-wise outlier detection (Sairanen et al., 2018); and correction for drift (Vos et al., 2017); motion, eddy, and susceptibility-induced distortions (Andersson et al., 2003; Andersson & Sotiropoulos, 2016); Gibbs ringing artefact (Kellner et al., 2016); bias field (Tustison et al., 2010); and gradient non-uniformities (Glasser et al., 2013; Rudrapatna et al., 2021). We performed multi-shell multi-tissue constrained spherical deconvolution (MSMT-CSD; Jeurissen et al. (2014)) and generated a whole-brain probabilistic tractogram seeding from the white matter comprising 3 million streamlines (Tournier et al., 2010).

We then applied COMMIT (Daducci et al., 2015, 2013) using a stick-zeppelin-ball model (Panagiotaki et al., 2012) to effectively filter out implausible connections while obtaining the intra-axonal signal fraction for each streamline, as described in Schiavi, Petracca, et al. (2020). For a set of fixed intra- and extra- axonal diffusivities, we assume that the IASF is constant along the streamline. To set the diffusivity parameters in COMMIT, we performed voxel-wise estimations in one younger participant (8-year-old female) and one older participant (17-year-old female). In the white matter, diffusivities had minimal variation between the younger and older participant (Table S1). As a result, for all subjects we set the following diffusivities $d_{par}=d_{par\_zep}=1.7\times10^{-3}$ mm^2/s, $d_{perp}=0.61\times10^{-3}$ mm^2/s, d_{iso} in $[1.7,3.0]\times10^{-3}$ mm^2/s for all participants.

For each subject, the connectomes were built using nodes from the individual T1-based parcellation by assigning the total IASF associated to each bundle as edge-weights as in Schiavi, Petracca, et al. (2020) and Gabusi et al. (2022). Briefly, for each subject, the microstructure-informed connectomes (i.e., obtained using COMMIT weights reflecting IASF associated to each streamline as entries) were built using the GM parcellation described above and computing the weighted average intra-axonal signal contribution of each bundle:

$$a_{ij} = \frac{\sum_{k=1}^{N_{ij}} x_{ij}^{k} \cdot l_k}{\frac{\sum_{k=1}^{N_{ij}} l_k}{N_{ij}}}$$

where i,j are the indices of ROIs connected by the bundle, N_{ij} is bundle's number of streamlines, x_{ij}^{k} is the weight of the streamline, k, obtained by COMMIT, and l_k, its length. In this way, each entry contained the total IASF associated to the bundle given by the weighted average of the streamline contribution multiplied by its length and divided by the average length of the bundle.

2.4. Network analysis

To investigate the relationship between network characteristics and age, we used the Brain Connectivity Toolbox for Python (Rubinov & Sporns, 2010) to compute the following weighted network measures:

- Modularity according to Newman's spectral community detection (Newman, 2013) with resolution parameter gamma=1;
- Global efficiency as the average of the inverse shortest path length (Rubinov & Sporns, 2010);
- Local efficiency as the global efficiency computed on the neighbourhood of the node (Rubinov & Sporns, 2010)
- Clustering coefficient as the mean of a node's clustering coefficient computed as the average intensity of triangles around each node; and
- Mean strength as the average of all the nodal strengths, computed as the sum of the weights of links connected to the node.

We computed these global network measures for the entire connectome, and again using smaller graphs containing only the nodes within each subnetwork of the Yeo7 atlas.

2.5. Age-relationships

To investigate age-related patterns of network characteristics across the eight Yeo7 networks and five lobes, we applied linear mixed effects modelling using lme4 (Bates et al., 2015) in R (RStudio v3.4.3). We built a linear model which included age (linear term), sex and Yeo7 network as predictors, with intracranial volume (ICV) included as a covariate. We examined four network characteristics (modularity, global efficiency, clustering coefficient, mean strength) and compared the fit of the standard linear model with alternative models that incorporated interaction terms. To identify the most appropriate model, we used the Akaike Information Criterion (AIC) (Akaike, 1974), selecting the model with the lowest AIC as the most parsimonious. Individual general linear models were run to determine age-related differences in specific network characteristics in all eight Yeo7 networks. Evidence for an association was deemed statistically significant when $p < .005$ (Benjamin et al., 2018).

2.6. Feature importance

To identify locally important nodes that contribute to developmental patterns within networks (identified in section 2.5), we performed age-prediction using linear regression and ElasticNet regularization in scikit-learn (i.e., L1 and L2 penalties). We investigated feature importance using the ROIs comprised in each network for age-prediction of local efficiency. First, we randomly split the data into training and validation sets using an 80-20 ratio, resulting in 80% of the data being allocated for training purposes and the remaining 20% for model evaluation (total N=88: 70 training; 18 testing). Then, we performed feature scaling to ensure that all variables were on a similar scale. To assess the generalization performance of the ElasticNet model and to prevent overfitting, we employed a 5-fold cross-validation approach. We performed a grid search to determine the optimal values for the L1 ratio ([0.1, 0.5, 0.7, 0.9, 0.95, 0.99, 1]) based on the regression coefficient (R^2).

The performance of the model was assessed using the validation dataset. Finally, the features with the largest weight coefficients were extracted to identify specific cortical regions driving age-relationships in local network efficiency.

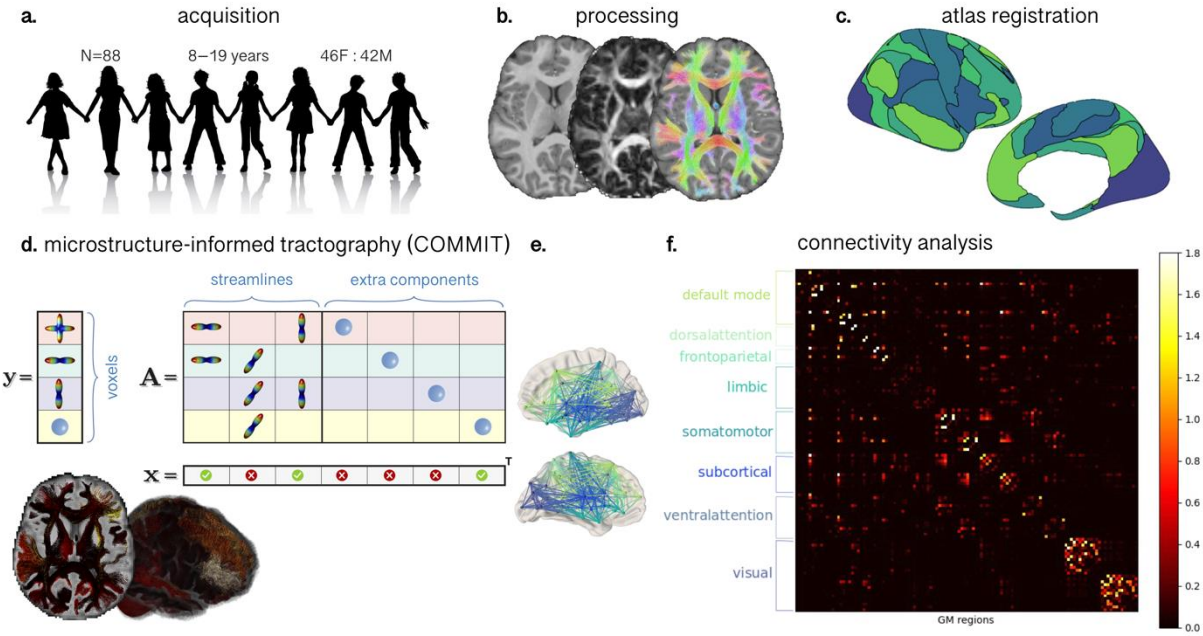

Figure 1: Workflow for constructing structural connectivity networks based on COMMIT derived streamline weights: a) MRI data were acquired on a 3T system with 300 mT/m gradients; b) T1 and dMRI data were pre-processed; c) canonical cortical networks derived from a functional atlas (Yeo et al., 2011) were co-registered to individual subject space; d) COMMIT (Daducci et al., 2015, 2013) was applied using a stick-zeppelin-ball model to filter out implausible connections, where computed weights reflect the intra-axonal signal fraction of each connection (brighter values = higher IASF); e) interconnected nodes coloured by canonical cortical network; f) connectivity matrix demonstrating connection strength between nodes within in each network (brighter values = higher IASF).

3. Results

3.1. Global network characteristics

Linear models revealed a positive relationship between age and modularity (R^2 = .08, p = .002), global efficiency (R^2 = 0.31, p < 0.001) and mean strength (R^2 = .38, p < .001) (Figure 2b). The relationship between age and clustering coefficient was not statistically significant (R^2 = .16, p = .02). As shown in the circle plot in Figure 2a, we also noted strong intra-regional connectivity

and strength within the visual and somatomotor networks, indicating robust interactions among regions within these networks.

To test whether specific networks were driving these developmental patterns of network properties, we tested age-by-network interactions using a linear mixed effects model. The various models tested, and the model selection results are summarised in Table S3. The best fitting model for all four graph measures included an age by network by sex interaction term. We observed significant age-by-network interactions in modularity ($F = 6.6$, $p < .001$), global efficiency ($F = 6.7$, $p < .001$), clustering coefficient ($F = 3.3$, $p = .002$), and mean strength ($F = 23.9$, $p < .001$). As these results indicated that there were age-related differences in network properties between the networks, we performed subsequent analyses to test for age associations within networks, to discern whether developmental patterns differed regionally. The various networks tested and their corresponding anatomical tractography depictions are illustrated in Figure 2c.

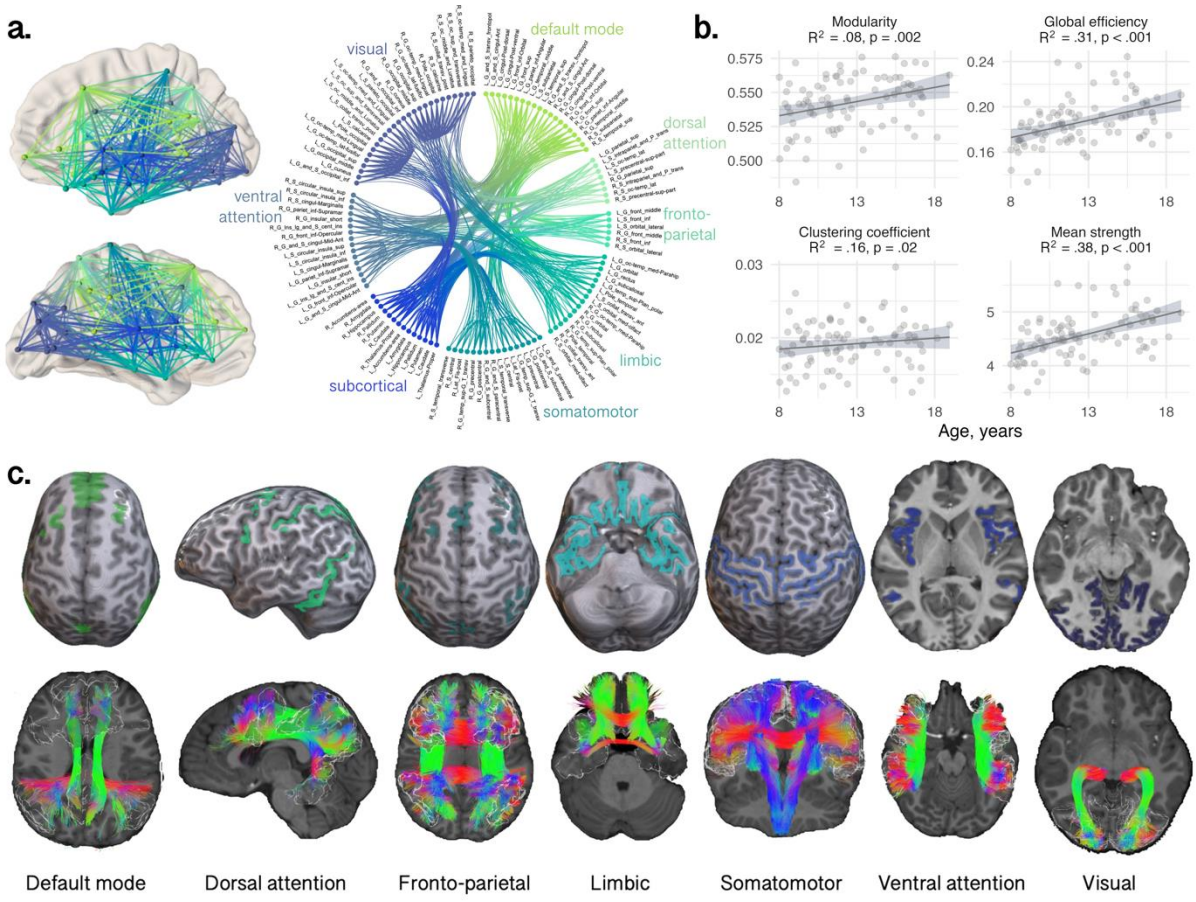

Figure 2: Relationship between age and global network measures computed for the whole connectome realized with Destrieux parcellation. a) Interconnected nodes obtained using the intra-axonal signal fraction estimated with COMMIT, coloured by canonical cortical network; b) Association between age and network characteristics between networks (R^2 and p-value); c) Depiction of atlas-derived cortical functional networks and representative white matter tracts traversing these networks, for an 8-year-old female participant.

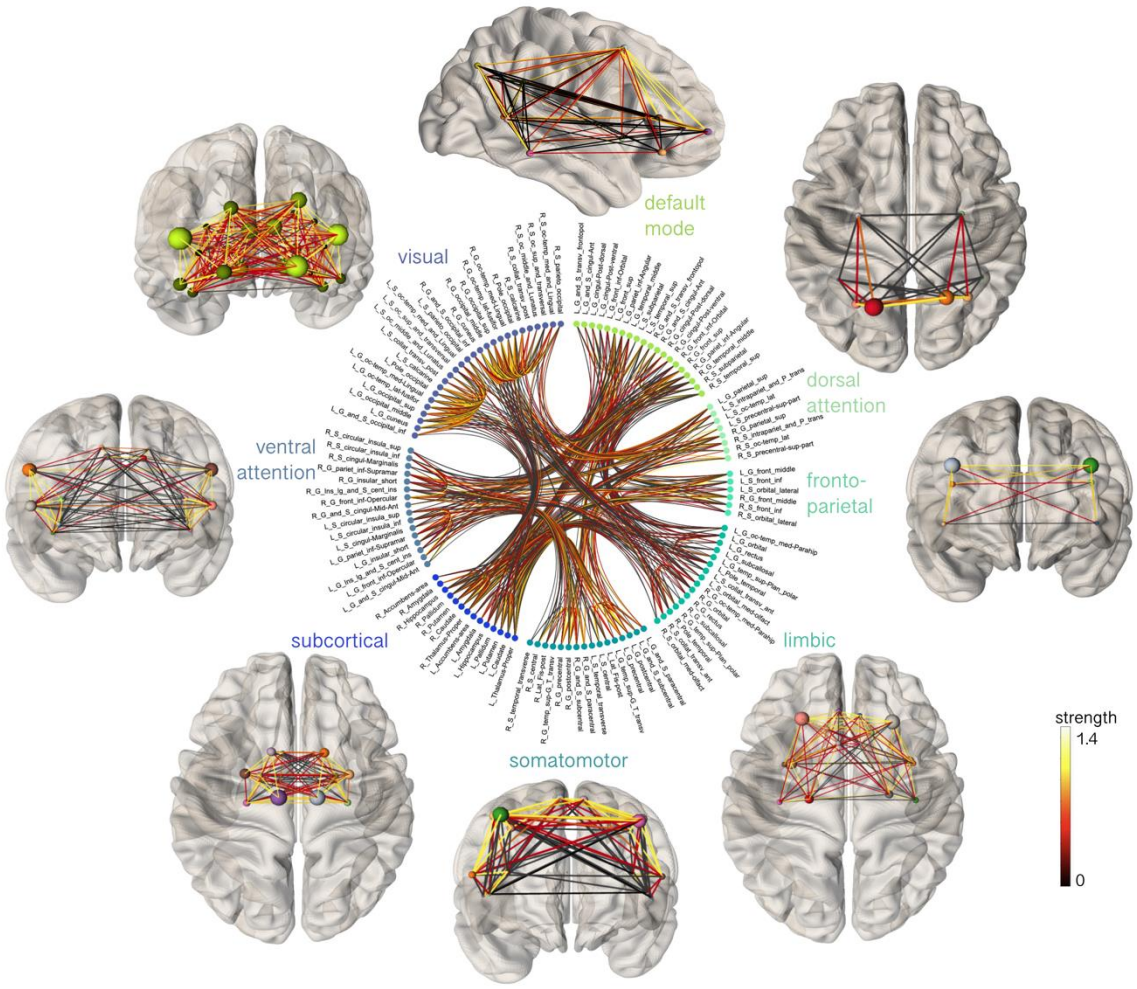

Figure 3: Spatial representation of the eight canonical cortical networks, with connections between nodes coloured by strength.

3.2. Sub-network characteristics

We identified regional differences in the age-related development of specific sub-networks (Table 1 and Figure 4). Through linear regression analyses within individual networks, we found statistically significant relationships between

age and global efficiency in the default mode (R^2 = .38, p = .001), somatomotor (R^2 = .28, p < .001) and visual networks (R^2 = .43, p < .001). Clustering coefficient was positively associated with age in the visual network (R^2 = .37, p < .001). Moreover, age exhibited a positive association with mean strength in the somatomotor network (R^2 = .33, p < .001) and the visual network (R^2 = .46, p < .001). We also observed a negative association between age and modularity in the ventral attention network (R^2 = .13, p < .001). These results were replicated when including connection density as a covariate to each linear model, with the additional correlation observed between clustering coefficient and age in the somatomotor network (R^2 = .63, p < .001; Table S4). Overall, our results highlight the distinct age-related developmental patterns in the visual and somatomotor networks.

Sex differences were observed, where males had higher clustering coefficient in the visual network (β[95%CI] = .67 [.29, 1.06], p=.0009), and higher mean strength in the default mode network (β[95%CI] = .71 [.34, 1.08], p=.0002), compared with females. Sex interactions (slope of M>F) were apparent in modularity of the limbic network (β[95%CI] = .74 [.31, 1.17], p=.0009).

To confirm that the age-dependence of visual network properties were significantly different from other networks, we performed linear mixed-effects modelling to discern whether age-by-network interactions were significantly different between the visual network and the seven remaining sub-networks. Where the age-relationship in the visual network was significantly stronger than each subsequent network, this is summarised in Table S5 and annotated in Table 1. In summary, the most marked observations were in network strength, where the visual network had a significantly stronger age-dependency compared to each individual network, apart from the somatomotor network which also had a positive relationship with age.

Table 1: Summary statistics for the relationship between age and global sub-network characteristics.

Network	Modularity		Global efficiency		Clustering coefficient		Mean strength	
	R^2	p-value	R^2	p-value	R^2	p-value	R^2	p-value
Default mode	.04	.55	.38	**.001**	.10	.59†	.43	.13†
Dorsal attention	-.03	.81	.06	.41†	.09	.20	.06	.23†

Fronto-parietal	.07	.66	.03	.58	-.01	.96	.07	.51†
Limbic	.07	.14	.19	.92	.14	.81	.21	.53†
Somatomotor	.01	.75	.28	**< .001**	.30	.20	.33	**< .001**
Subcortical	.08	.27	.03	.26	.01	.72	.02	.47†
Ventral attention	.13	**< .001**	.19	.006	.11	.47†	.22	.12†
Visual	.11	.17	.43	**< .001**	.37	**< .001**	.46	**< .001**

Note: Adjusted R^2 determined using a linear model including age, sex and total intracranial volume. Bold values indicate p<.005. † denotes a significant difference in the slope of the age relationship compared with the visual network.

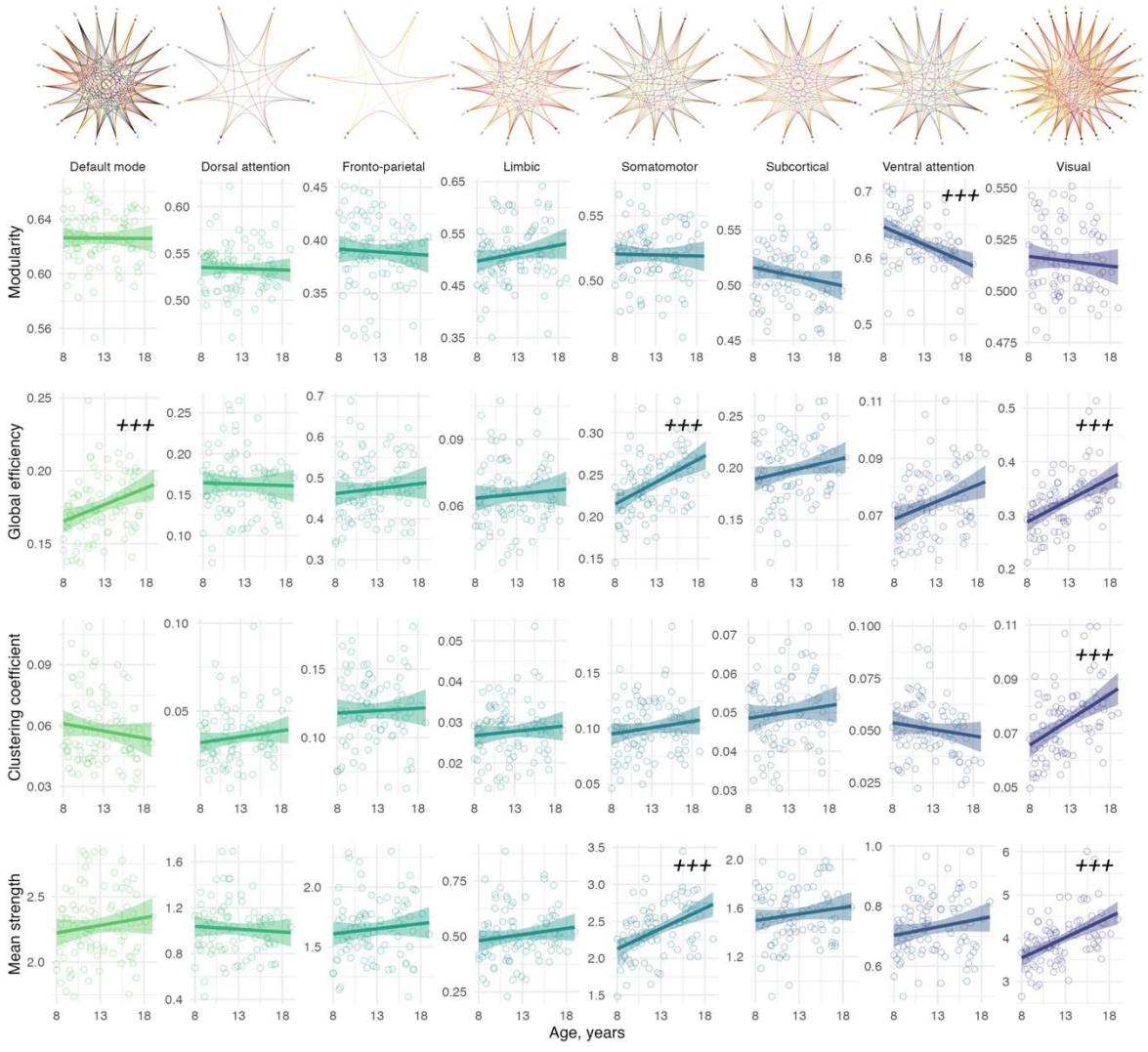

Figure 4: Association between age and network properties within sub-networks. Significant age relationships are annotated (+++: p<.005). Top panel represents circle plots of within-network nodes, with brighter yellow connections indicative of higher mean strength. Nodes within the circle plots are labelled by number (see Table S2).

3.3. Feature importance of local efficiency

Age prediction of local efficiency in the visual network yielded a regression coefficient of 0.45 (RMSE: 2.2, p=.001, Figure 5a) on the validation set (optimal value for L1=0.1). Feature importance in the visual network identified specific nodes (Figure 5) driving age-related increases in local efficiency. The 10 most sensitive nodes were balanced between hemispheres (5 nodes in right hemisphere, and 5 in the left) and accounted for 75% of variation in total weights (of a total of 26 nodes). Figure 5b summarises the regions ranked by weight, and Figure 5c depicts these regions in axial, sagittal and coronal views in 3D. Nodes with high feature importance for age clustered together, including nodes which form the dorsal (left superior occipital gyrus and middle occipital gyrus and sulcus) and the ventral (right medial occipito-temporal sulcus and gyrus, and right lingual gyrus) visual pathways.

Age prediction for local efficiency of the somatomotor network yielded a weaker regression coefficient of 0.10 which was not statistically significant (p=.10). Feature importance identified specific regions driving age-related increases in local efficiency. Six nodes balanced between hemispheres (3 nodes in right hemisphere, and 3 in the left) accounted for 70% of the variation in total weights (of a total of 16 nodes). Nodes with high feature importance for age included the bilateral precentral gyrus, right postcentral gyrus, bilateral central sulcus, and left transverse temporal gyrus.

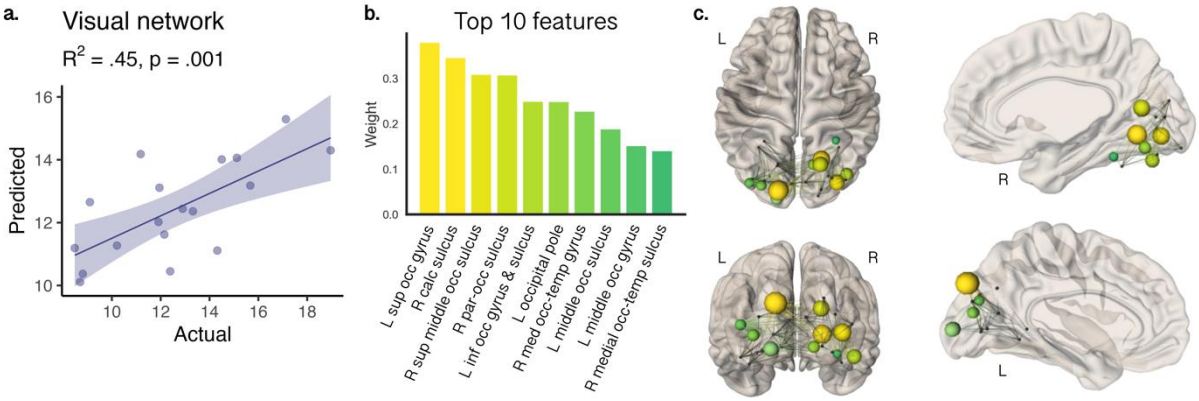

Figure 5: Feature importance for age-prediction of local network efficiency in the visual cortex. A) predicted age was significantly associated with actual age; B) top 10 ranking regions that contributed most to age-related patterns

displayed on C) axial, sagittal, and coronal glass brain views, where nodes are scaled and color-coded by weight. Nodes with high feature importance included left superior and middle occipital gyrus and right medial occipito-temporal gyrus.

4. Discussion

We used microstructure-informed tractography to investigate global and local network characteristics in canonical cortical networks among a group of typically developing children and adolescents. Our study revealed three main findings:

First, whole-brain network-based measures of modularity, global efficiency and mean strength increased with age. This indicates that as children move through adolescence, the shortest path between nodes (in this case, regions from the Destrieux parcellation) decreases, resulting in a more efficient transfer of information. As a result, the nodes tend to cluster together to form hubs, and the strength of each white matter connection increases with age. These findings align with known age-related increases in global efficiency during adolescent development (Baker et al., 2015; Khundrakpam et al., 2013; Koenis et al., 2018; Van den Heuvel & Sporns, 2013). Additionally, previous white matter studies have shown substantial increases in intra-axonal signal fraction with age (Chang et al., 2015; Genc et al., 2020; Palmer et al., 2022), aligning with our observations of age-related increases in mean strength.

Second, sub-network analyses revealed specific networks with substantial age-related differences occurring from childhood to adolescence. In the default mode, somatomotor, and visual networks, global efficiency was higher with older age. Additionally, clustering coefficient was higher with age in the visual network, and mean strength was higher with age in the somatomotor and visual networks. Notably, brain structures, such as the primary visual and somatomotor cortex have highly organized and specialized structures that are closely related to their function, such as discriminating visual features (Wandell, 1999) and performing specific motor functions (Gordon et al., 2023).

Together, our findings of age-related maturation of network efficiency and strength suggests a high degree of integration and communication within motor and visual processing regions, potentially reflecting the ongoing maturation of visual information processing and motor coordination capabilities during development. Our specific findings in the visual network align with previously observed temporal patterns of white matter microstructural maturation in the visual cortex (Colby et al., 2011; Genc et al., 2017) which are likely to be closely linked to age-related increases in axon density in humans (Genc et al., 2020) and rodents (Juraska & Willing, 2017).

Age-prediction in the visual cortex pointed to a smaller cluster of five regions per hemisphere that contributed to >75% of the observed age-related differences in local network efficiency. Our data driven approach suggests that connections between nodes in the left dorsal (middle and superior occipital) visual pathway and the right ventral (middle occipito-temporal) visual pathway are driving developmental improvements in local network efficiency. The visual system undergoes early establishment during prenatal development and continues to mature through life (Gogtay et al., 2004; Knudsen, 2004). While myelination in the visual cortex is largely completed by the first year of life (Deoni et al., 2015), recent research indicates that myelination follows a protracted course in ventral temporal cortices (Natu et al., 2019). Ongoing intra-cortical myelination of the ventral temporal cortex may underlie MRI-derived estimates of cortical thinning, previously attributed to synaptic pruning (Gomez et al., 2017; Natu et al., 2019).

The maturation of association visual cortices supports higher level visual processing (e.g. recognising and discriminating objects, motion perception etc.) (Gomez et al., 2018). Our findings align with task-based fMRI studies involving object and shape recognition tasks, which demonstrate protracted development of dorsal and ventral visual pathways (Freud et al., 2019; Ward et al., 2023). These developmental improvements in shape-processing mechanisms likely contribute to microstructure-specific strengthening of global network efficiency and strength of white matter connections within the visual network through child and adolescent brain development. The age-related increases in local network efficiency in lateral temporo-occipital cortices may facilitate improvements in visual processing and function between these association cortices.

The myelination of these visual pathways may help to refine and optimize the neural connections and improve visual processing capabilities. Whilst we did not directly study myelination here, the intra-axonal signal fraction explains a significant proportion of the age-related variance in network efficiency and connection strength. Taken together, our findings suggest that white matter connections within the visual cortex undergoes protracted development through childhood and adolescence. While our study primarily focuses on white matter microstructure for exploring graph-based measures, our observations of higher efficiency and connection strength with older age is predominantly due to ongoing microstructural maturation in the visual cortex.

4.1. Methodological advantages of the current approach

We employed a data-driven approach to establish correspondence between a structural parcellation and functional atlas in each participant (Baum et al., 2017). This involved selecting the maximum number of voxels in the intersection between a smaller cortical region with its corresponding larger functional network. By ensuring that this overlap was consistent with the homologous ROIs and in at least 80% of the participants, we generated canonical cortical networks for the basis of regional graph-based analyses.

One of the significant advantages of the COMMIT framework is its ability to assign specific microstructural properties to individual tractography-reconstructed streamlines, which sets it apart from conventional (voxel-wise or vertex-wise) approaches. Without taking these factors into account, complex intra-voxel heterogeneity (Schilling et al., 2022) and nodal size (Danielle S. Bassett et al., 2011) can bias estimates. By allowing a distribution of microstructural values to be assigned to a voxel, i.e., the number of values is equal to the number of unique streamlines passing through the voxel and retained for analysis, COMMIT offers a more quantitative estimation of network properties. In the context of graph theory, we can capture the dynamic strengthening and weakening of connections based on their underlying microstructure, known to mature rapidly through childhood and adolescence.

Indeed, when repeating the analysis of age-related differences in network properties using the reconstructed number of streamlines (NOS) as edge-weights, we observed differences in results. Age-related increases in network properties were present in the fronto-parietal and somatomotor networks but absent from the visual and default mode networks (Table S7). Upon further

investigation, we observed a significant positive relationship between age and the number of reconstructed streamlines in the fronto-parietal and somatomotor networks (Table S8) – suggesting that the total NOS may be driving these age-related increases in network properties. Various factors unrelated to the underlying microstructure, such as tract shape, length and curvature, can impact the number of streamlines reconstructed (Derek K Jones et al., 2013; Maier-Hein et al., 2017). One example is depicted in Figure 2c; in the visual network the Meyer's loop of the optic radiation contains fibres which undergo large turns, which can result in a smaller number of valid streamlines recovered by tractography and many false positives (Chamberland et al., 2018). As such, we need to exercise caution when interpreting results using connectomes weighted by NOS.

Overall, the COMMIT framework offers a nuanced and detailed characterization of microstructural properties along individual streamlines, countering complex intra-voxel heterogeneity, making it a powerful tool for a more meaningful assessment of brain connectivity (Gabusi et al., 2022; Schiavi et al., 2022; Schiavi, Ocampo-Pineda, et al., 2020; Schiavi, Petracca, et al., 2020).

4.2. Limitations and future directions

It is important to acknowledge that certain functional networks utilised in our study here contain fewer nodes than others, potentially influencing our interpretations. Although we adopted a robust method to generate reproducible cortical nodes for each functional network, it resulted in some networks having a small number of nodes. Using a parcellation method with finer granularity (Glasser et al., 2016; Schaefer et al., 2017) and replicating analyses in a larger independent cohort such as the adolescent brain development cohort (Casey et al., 2018) would be warranted.

While there is a certain relationship between brain structure and function, structure-function coupling occurs in a spatially-dependent hierarchical manner (Baum et al., 2020). The brain is a complex and dynamic organ, with function influenced by a variety of factors, including structural organisation (Chamberland et al., 2017) and neural activity. Combining task-based or resting-state fMRI with microstructure-informed connectomes may better elucidate structure-function coupling across the developing brain (Suárez et al., 2020).

Despite running a 'gold-standard' dMRI pre-processing pipeline, susceptibility-induced distortion artefacts may introduce an additional source of variance into the diffusion MRI data, especially in fronto-parietal regions with an air/bone interface such as the nasal cavity. Whilst the aforementioned factors may help explain why we did not observe an age dependence of network-based measures of brain connectivity in regions known to remodel in adolescence (e.g. the fronto-parietal network), it is known that functional networks that are in close range demonstrate stronger white matter connectivity (Hermundstad et al., 2013), which may explain why our findings of global efficiency and mean strength were confined to the somatomotor and visual networks. Future work could involve examining changes in edge weight and connection density of short vs long-range connections in younger vs older participants which might reveal other interesting changes in topology.

Finally, new frontiers in characterising the developing connectome using biologically meaningful mathematical models of brain connections are promising (Akarca et al., 2023; Seguin et al., 2023). Recent updates to the COMMIT framework offer the opportunity to incorporate additional imaging contrasts, such as myelin-sensitive contrasts, leading to improved delineation of anatomically accurate whole-brain tractography (Leppert et al., 2023; Schiavi et al., 2022).

5. Conclusion

Incorporating microstructural information into network analyses has shed light on distinct regional age-related development of brain networks. Notably, we observed unique characteristics within the visual network throughout development, supporting its ongoing maturation, reaffirming previously reported patterns of protracted development in the dorsal and ventral visual pathways. Overall, our study demonstrates the power of microstructure-informed tractography to decipher intricate developmental patterns, reinforcing the potential for deepening our understanding of brain connectivity and development.

6. Supporting information

Acknowledgments

We are grateful to the participants and their families for their participation in this study. We thank Umesh Rudrapatna and John Evans for their support with image acquisition protocols, Isobel Ward for assistance with data collection, Joseph Yang for scientific discussions, and Greg Parker for contributions to data pre-processing and model fitting pipelines. Image credit (Figure 1a) by kjpargeter on Freepik.

Funding

The data were acquired at the UK National Facility for In Vivo MR Imaging of Human Tissue Microstructure funded by the EPSRC (grant EP/M029778/1), and The Wolfson Foundation.
SG received positional funding from the Royal Children's Hospital Foundation (RCHF 2022-1402). SS received funding from the University of Verona Internationalisation Programme 2019 (Action 4C). This research was funded in whole, or in part, by a Wellcome Trust Investigator Award (096646/Z/11/Z) and a Wellcome Trust Strategic Award (104943/Z/14/Z). CMWT was supported by a Veni grant (17331) from the Dutch Research Council (NWO) and the Wellcome Trust [215944/Z/19/Z].

SG acknowledges the support of the Royal Children's Hospital, Murdoch Children's Research Institute, The University of Melbourne Department of Paediatrics, and the Victorian Government's Operational Infrastructure Support Program.

Authors' Contributions

S.S., S.G. and D.K.J. conceptualized the problem. S.S., S.G., M.C. and C.T. analyzed the MRI data. S.G. and E.R. acquired all MRI data. S.G and M.C. performed statistical analyses. A.D. and D.J., supervised and raised funding for this project. S.S., S.G. and D.K.J. wrote the original draft of the manuscript. S.S., S.G., M.C., C.T., E.R., A.D., and D.K.J. reviewed and edited the manuscript.

Code and data availability

The code for COMMIT is open source and freely available at https://github.com/daducci/COMMIT.

Disclosures

Declarations of interest: SG, MC, CT, ER, AD, DKJ declare no conflict of interest. SS is employed by ASG Superconductors S.p.A. but there is no financial interest related to this work.

7. References

Akaike, H. (1974). A new look at the statistical model identification. *IEEE Transactions on Automatic Control*, *19*(6), 716-723. https://doi.org/10.1109/TAC.1974.1100705

Akarca, D., Schiavi, S., Achterberg, J., Genc, S., Jones, D., & Astle, D. (2023). A weighted generative model of the human connectome. *bioRxiv*, 2023.2006.2023.546237. https://doi.org/10.1101/2023.06.23.546237

Andersson, J. L., Skare, S., & Ashburner, J. (2003). How to correct susceptibility distortions in spin-echo echo-planar images: application to diffusion tensor imaging. *NeuroImage*, *20*(2), 870-888.

Andersson, J. L. R., & Sotiropoulos, S. N. (2016). An integrated approach to correction for off-resonance effects and subject movement in diffusion MR imaging. *NeuroImage*, *125*, 1063-1078. https://doi.org/10.1016/j.neuroimage.2015.10.019

Avants, B. B., Tustison, N. J., Song, G., Cook, P. A., Klein, A., & Gee, J. C. (2011). A reproducible evaluation of ANTs similarity metric performance in brain image registration. *NeuroImage*, *54*(3), 2033-2044.

Baker, S. T., Lubman, D. I., Yücel, M., Allen, N. B., Whittle, S., Fulcher, B. D., Zalesky, A., & Fornito, A. (2015). Developmental changes in brain network hub connectivity in late adolescence. *Journal of Neuroscience*, *35*(24), 9078-9087.

Bartzokis, G., Lu, P. H., Heydari, P., Couvrette, A., Lee, G. J., Kalashyan, G., Freeman, F., Grinstead, J. W., Villablanca, P., Finn, J. P., Mintz, J., Alger, J. R., & Altshuler, L. L. (2012). Multimodal magnetic resonance imaging assessment of white matter aging trajectories over the lifespan of healthy individuals. *Biol Psychiatry*, *72*(12), 1026-1034. https://doi.org/10.1016/j.biopsych.2012.07.010

Bassett, D. S., Brown, J. A., Deshpande, V., Carlson, J. M., & Grafton, S. T. (2011). Conserved and variable architecture of human white matter connectivity. *NeuroImage*, *54*(2), 1262-1279. https://doi.org/https://doi.org/10.1016/j.neuroimage.2010.09.006

Bassett, D. S., Wymbs, N. F., Porter, M. A., Mucha, P. J., Carlson, J. M., & Grafton, S. T. (2011). Dynamic reconfiguration of human brain networks during learning. *Proceedings of the National Academy of Sciences*, *108*(18), 7641-7646.

Bates, D., Kliegl, R., Vasishth, S., & Baayen, H. (2015). Parsimonious mixed models. *arXiv preprint arXiv:1506.04967*.

Baum, G. L., Ciric, R., Roalf, D. R., Betzel, R. F., Moore, T. M., Shinohara, R. T., Kahn, A. E., Vandekar, S. N., Rupert, P. E., Quarmley, M., Cook, P. A., Elliott, M. A., Ruparel, K., Gur, R. E., Gur, R. C., Bassett, D. S., & Satterthwaite, T. D. (2017). Modular

Segregation of Structural Brain Networks Supports the Development of Executive Function in Youth. *Curr Biol*, *27*(11), 1561-1572.e1568. https://doi.org/10.1016/j.cub.2017.04.051

Baum, G. L., Cui, Z., Roalf, D. R., Ciric, R., Betzel, R. F., Larsen, B., Cieslak, M., Cook, P. A., Xia, C. H., Moore, T. M., Ruparel, K., Oathes, D. J., Alexander-Bloch, A. F., Shinohara, R. T., Raznahan, A., Gur, R. E., Gur, R. C., Bassett, D. S., & Satterthwaite, T. D. (2020). Development of structure–function coupling in human brain networks during youth. *Proceedings of the National Academy of Sciences*, *117*(1), 771-778. https://doi.org/10.1073/pnas.1912034117

Bells, S., Cercignani, M., Deoni, S., Assaf, Y., Pasternak, O., Evans, C., Leemans, A., & Jones, D. (2011). Tractometry–comprehensive multi-modal quantitative assessment of white matter along specific tracts. Proc. ISMRM,

Benjamin, D. J., Berger, J. O., Johannesson, M., Nosek, B. A., Wagenmakers, E. J., Berk, R., Bollen, K. A., Brembs, B., Brown, L., Camerer, C., Cesarini, D., Chambers, C. D., Clyde, M., Cook, T. D., De Boeck, P., Dienes, Z., Dreber, A., Easwaran, K., Efferson, C., Fehr, E., Fidler, F., Field, A. P., Forster, M., George, E. I., Gonzalez, R., Goodman, S., Green, E., Green, D. P., Greenwald, A. G., Hadfield, J. D., Hedges, L. V., Held, L., Hua Ho, T., Hoijtink, H., Hruschka, D. J., Imai, K., Imbens, G., Ioannidis, J. P. A., Jeon, M., Jones, J. H., Kirchler, M., Laibson, D., List, J., Little, R., Lupia, A., Machery, E., Maxwell, S. E., McCarthy, M., Moore, D. A., Morgan, S. L., Munafó, M., Nakagawa, S., Nyhan, B., Parker, T. H., Pericchi, L., Perugini, M., Rouder, J., Rousseau, J., Savalei, V., Schönbrodt, F. D., Sellke, T., Sinclair, B., Tingley, D., Van Zandt, T., Vazire, S., Watts, D. J., Winship, C., Wolpert, R. L., Xie, Y., Young, C., Zinman, J., & Johnson, V. E. (2018). Redefine statistical significance. *Nature Human Behaviour*, *2*(1), 6-10. https://doi.org/10.1038/s41562-017-0189-z

Bergamino, M., Schiavi, S., Daducci, A., Walsh, R. R., & Stokes, A. M. (2022). Analysis of brain structural connectivity networks and white matter integrity in patients with mild cognitive impairment. *Frontiers in Aging Neuroscience*, *14*, 793991.

Blakemore, S. J., & Choudhury, S. (2006). Development of the adolescent brain: implications for executive function and social cognition. *Journal of child psychology and psychiatry*, *47*(3‐4), 296-312.

Casey, B. J., Cannonier, T., Conley, M. I., Cohen, A. O., Barch, D. M., Heitzeg, M. M., Soules, M. E., Teslovich, T., Dellarco, D. V., Garavan, H., Orr, C. A., Wager, T. D., Banich, M. T., Speer, N. K., Sutherland, M. T., Riedel, M. C., Dick, A. S., Bjork, J. M., Thomas, K. M., Chaarani, B., Mejia, M. H., Hagler, D. J., Daniela Cornejo, M., Sicat, C. S., Harms, M. P., Dosenbach, N. U. F., Rosenberg, M., Earl, E., Bartsch, H., Watts, R., Polimeni, J. R., Kuperman, J. M., Fair, D. A., & Dale, A. M. (2018). The Adolescent Brain Cognitive Development (ABCD) study: Imaging acquisition across 21 sites. *Developmental Cognitive Neuroscience*, *32*, 43-54. https://doi.org/https://doi.org/10.1016/j.dcn.2018.03.001

Chamberland, M., Girard, G., Bernier, M., Fortin, D., Descoteaux, M., & Whittingstall, K. (2017). On the Origin of Individual Functional Connectivity Variability: The Role of White Matter Architecture. *Brain Connectivity*, *7*(8), 491-503. https://doi.org/10.1089/brain.2017.0539

Chamberland, M., Raven, E. P., Genc, S., Duffy, K., Descoteaux, M., Parker, G. D., Tax, C. M. W., & Jones, D. K. (2019). Dimensionality reduction of diffusion MRI measures for improved tractometry of the human brain. *NeuroImage*, *200*, 89-100. https://doi.org/10.1016/j.neuroimage.2019.06.020

765 Chamberland, M., Tax, C. M. W., & Jones, D. K. (2018). Meyer's loop tractography for
766 image-guided surgery depends on imaging protocol and hardware. *NeuroImage:*
767 *Clinical*, *20*, 458-465. https://doi.org/https://doi.org/10.1016/j.nicl.2018.08.021
768 Chang, Y. S., Owen, J. P., Pojman, N. J., Thieu, T., Bukshpun, P., Wakahiro, M. L. J.,
769 Berman, J. I., Roberts, T. P. L., Nagarajan, S. S., Sherr, E. H., & Mukherjee, P.
770 (2015). White Matter Changes of Neurite Density and Fiber Orientation Dispersion
771 during Human Brain Maturation. *PLOS ONE*, *10*(6), e0123656.
772 https://doi.org/10.1371/journal.pone.0123656
773 Colby, J. B., Van Horn, J. D., & Sowell, E. R. (2011). Quantitative in vivo evidence for broad
774 regional gradients in the timing of white matter maturation during adolescence.
775 *NeuroImage*, *54*(1), 25-31.
776 https://doi.org/https://doi.org/10.1016/j.neuroimage.2010.08.014
777 Daducci, A., Dal Palù, A., Lemkaddem, A., & Thiran, J. P. (2015). COMMIT: Convex
778 optimization modeling for microstructure informed tractography. *IEEE Trans Med*
779 *Imaging*, *34*(1), 246-257. https://doi.org/10.1109/tmi.2014.2352414
780 Daducci, A., Palù, A. D., Lemkaddem, A., & Thiran, J. P. (2013, 7-11 April 2013). A convex
781 optimization framework for global tractography. 2013 IEEE 10th International
782 Symposium on Biomedical Imaging,
783 Deoni, S. C. L., Dean, D. C., Remer, J., Dirks, H., & O'Muircheartaigh, J. (2015). Cortical
784 maturation and myelination in healthy toddlers and young children. *NeuroImage*, *115*,
785 147-161. https://doi.org/https://doi.org/10.1016/j.neuroimage.2015.04.058
786 Desikan, R. S., Ségonne, F., Fischl, B., Quinn, B. T., Dickerson, B. C., Blacker, D., Buckner,
787 R. L., Dale, A. M., Maguire, R. P., & Hyman, B. T. (2006). An automated labeling
788 system for subdividing the human cerebral cortex on MRI scans into gyral based
789 regions of interest. *NeuroImage*, *31*(3), 968-980.
790 Destrieux, C., Fischl, B., Dale, A., & Halgren, E. (2010). Automatic parcellation of human
791 cortical gyri and sulci using standard anatomical nomenclature. *NeuroImage*, *53*(1), 1-
792 15.
793 Fornito, A., Zalesky, A., & Bullmore, E. (2016). *Fundamentals of brain network analysis*.
794 Academic press.
795 Freud, E., Plaut, D. C., & Behrmann, M. (2019). Protracted Developmental Trajectory of
796 Shape Processing along the Two Visual Pathways. *J Cogn Neurosci*, *31*(10), 1589-
797 1597. https://doi.org/10.1162/jocn_a_01434
798 Gabusi, I., Pontillo, G., Petracca, M., Battocchio, M., Bosticardo, S., Costabile, T., Daducci,
799 A., Pane, C., Riccio, E., & Pisani, A. (2022). Structural disconnection and functional
800 reorganization in Fabry disease: a multimodal MRI study. *Brain Communications*,
801 *4*(4), fcac187.
802 Geeraert, B. L., Lebel, R. M., & Lebel, C. (2019). A multiparametric analysis of white matter
803 maturation during late childhood and adolescence. *Human Brain Mapping*, *0*(0).
804 https://doi.org/10.1002/hbm.24706
805 Genc, S., Raven, E. P., Drakesmith, M., Blakemore, S.-J., & Jones, D. K. (2023). Novel
806 insights into axon diameter and myelin content in late childhood and adolescence.
807 *Cerebral Cortex*, *33*(10), 6435-6448. https://doi.org/10.1093/cercor/bhac515
808 Genc, S., Seal, M. L., Dhollander, T., Malpas, C. B., Hazell, P., & Silk, T. J. (2017). White
809 matter alterations at pubertal onset. *NeuroImage*, *156*, 286-292.
810 https://doi.org/10.1016/j.neuroimage.2017.05.017
811 Genc, S., Smith, R. E., Malpas, C. B., Anderson, V., Nicholson, J. M., Efron, D., Sciberras,
812 E., Seal, M. L., & Silk, T. J. (2018). Development of white matter fibre density and
813 morphology over childhood: A longitudinal fixel-based analysis. *NeuroImage*, *183*,
814 666-676. https://doi.org/10.1016/j.neuroimage.2018.08.043

Genc, S., Tax, C. M. W., Raven, E. P., Chamberland, M., Parker, G. D., & Jones, D. K. (2020). Impact of b-value on estimates of apparent fibre density. *Human Brain Mapping*, *41*(10), 2583-2595. https://doi.org/10.1002/hbm.24964

Giedd, J. N., Blumenthal, J., Jeffries, N. O., Castellanos, F. X., Liu, H., Zijdenbos, A., Paus, T., Evans, A. C., & Rapoport, J. L. (1999). Brain development during childhood and adolescence: a longitudinal MRI study. *Nat Neurosci*, *2*(10), 861-863. https://doi.org/10.1038/13158

Glasser, M. F., Coalson, T. S., Robinson, E. C., Hacker, C. D., Harwell, J., Yacoub, E., Ugurbil, K., Andersson, J., Beckmann, C. F., Jenkinson, M., Smith, S. M., & Van Essen, D. C. (2016). A multi-modal parcellation of human cerebral cortex. *Nature*, *536*(7615), 171-178. https://doi.org/10.1038/nature18933

Glasser, M. F., Sotiropoulos, S. N., Wilson, J. A., Coalson, T. S., Fischl, B., Andersson, J. L., Xu, J., Jbabdi, S., Webster, M., Polimeni, J. R., Van Essen, D. C., & Jenkinson, M. (2013). The minimal preprocessing pipelines for the Human Connectome Project. *NeuroImage*, *80*, 105-124. https://doi.org/10.1016/j.neuroimage.2013.04.127

Gogtay, N., Giedd, J. N., Lusk, L., Hayashi, K. M., Greenstein, D., Vaituzis, A. C., Nugent, T. F., Herman, D. H., Clasen, L. S., Toga, A. W., Rapoport, J. L., & Thompson, P. M. (2004). Dynamic mapping of human cortical development during childhood through early adulthood. *Proceedings of the National Academy of Sciences*, *101*(21), 8174-8179. https://doi.org/10.1073/pnas.0402680101

Gomez, J., Barnett, M. A., Natu, V., Mezer, A., Palomero-Gallagher, N., Weiner, K. S., Amunts, K., Zilles, K., & Grill-Spector, K. (2017). Microstructural proliferation in human cortex is coupled with the development of face processing. *Science*, *355*(6320), 68-71. https://doi.org/10.1126/science.aag0311

Gomez, J., Natu, V., Jeska, B., Barnett, M., & Grill-Spector, K. (2018). Development differentially sculpts receptive fields across early and high-level human visual cortex. *Nature Communications*, *9*(1), 788. https://doi.org/10.1038/s41467-018-03166-3

Gordon, E. M., Chauvin, R. J., Van, A. N., Rajesh, A., Nielsen, A., Newbold, D. J., Lynch, C. J., Seider, N. A., Krimmel, S. R., Scheidter, K. M., Monk, J., Miller, R. L., Metoki, A., Montez, D. F., Zheng, A., Elbau, I., Madison, T., Nishino, T., Myers, M. J., Kaplan, S., Badke D'Andrea, C., Demeter, D. V., Feigelis, M., Ramirez, J. S. B., Xu, T., Barch, D. M., Smyser, C. D., Rogers, C. E., Zimmermann, J., Botteron, K. N., Pruett, J. R., Willie, J. T., Brunner, P., Shimony, J. S., Kay, B. P., Marek, S., Norris, S. A., Gratton, C., Sylvester, C. M., Power, J. D., Liston, C., Greene, D. J., Roland, J. L., Petersen, S. E., Raichle, M. E., Laumann, T. O., Fair, D. A., & Dosenbach, N. U. F. (2023). A somato-cognitive action network alternates with effector regions in motor cortex. *Nature*, *617*(7960), 351-359. https://doi.org/10.1038/s41586-023-05964-2

Grayson, D. S., & Fair, D. A. (2017). Development of large-scale functional networks from birth to adulthood: A guide to the neuroimaging literature. *NeuroImage*, *160*, 15-31.

Greve, D. N., & Fischl, B. (2009). Accurate and robust brain image alignment using boundary-based registration. *NeuroImage*, *48*(1), 63-72.

Gu, S., Satterthwaite, T. D., Medaglia, J. D., Yang, M., Gur, R. E., Gur, R. C., & Bassett, D. S. (2015). Emergence of system roles in normative neurodevelopment. *Proceedings of the National Academy of Sciences*, *112*(44), 13681-13686.

Hagmann, P., Kurant, M., Gigandet, X., Thiran, P., Wedeen, V. J., Meuli, R., & Thiran, J.-P. (2007). Mapping Human Whole-Brain Structural Networks with Diffusion MRI. *PLOS ONE*, *2*(7), e597. https://doi.org/10.1371/journal.pone.0000597

Hermundstad, A. M., Bassett, D. S., Brown, K. S., Aminoff, E. M., Clewett, D., Freeman, S., Frithsen, A., Johnson, A., Tipper, C. M., Miller, M. B., Grafton, S. T., & Carlson, J.

M. (2013). Structural foundations of resting-state and task-based functional connectivity in the human brain. *Proceedings of the National Academy of Sciences*, *110*(15), 6169-6174. https://doi.org/10.1073/pnas.1219562110

Herting, M. M., Kim, R., Uban, K. A., Kan, E., Binley, A., & Sowell, E. R. (2017). Longitudinal changes in pubertal maturation and white matter microstructure. *Psychoneuroendocrinology*, *81*, 70-79. https://doi.org/10.1016/j.psyneuen.2017.03.017

Jenkinson, M., Bannister, P., Brady, M., & Smith, S. (2002). Improved optimization for the robust and accurate linear registration and motion correction of brain images. *NeuroImage*, *17*(2), 825-841.

Jeurissen, B., Leemans, A., Tournier, J. D., Jones, D. K., & Sijbers, J. (2013). Investigating the prevalence of complex fiber configurations in white matter tissue with diffusion magnetic resonance imaging. *Hum Brain Mapp*, *34*(11), 2747-2766. https://doi.org/10.1002/hbm.22099

Jeurissen, B., Tournier, J. D., Dhollander, T., Connelly, A., & Sijbers, J. (2014). Multi-tissue constrained spherical deconvolution for improved analysis of multi-shell diffusion MRI data. *NeuroImage*, *103*, 411-426. https://doi.org/10.1016/j.neuroimage.2014.07.061

Jones, D. K., Catani, M., Pierpaoli, C., Reeves, S. J., Shergill, S. S., O'Sullivan, M., Golesworthy, P., McGuire, P., Horsfield, M. A., & Simmons, A. (2006). Age effects on diffusion tensor magnetic resonance imaging tractography measures of frontal cortex connections in schizophrenia. *Human Brain Mapping*, *27*(3), 230-238.

Jones, D. K., Knösche, T. R., & Turner, R. (2013). White matter integrity, fiber count, and other fallacies: the do's and don'ts of diffusion MRI. *NeuroImage*, *73*, 239-254.

Jones, D. K., Knösche, T. R., & Turner, R. (2013). White matter integrity, fiber count, and other fallacies: the do's and don'ts of diffusion MRI. *NeuroImage*, *73*, 239-254. https://doi.org/10.1016/j.neuroimage.2012.06.081

Juraska, J. M., & Willing, J. (2017). Pubertal onset as a critical transition for neural development and cognition. *Brain Res*, *1654*, 87-94. https://doi.org/https://doi.org/10.1016/j.brainres.2016.04.012

Kanaan, R. A., Shergill, S. S., Barker, G. J., Catani, M., Ng, V. W., Howard, R., McGuire, P. K., & Jones, D. K. (2006). Tract-specific anisotropy measurements in diffusion tensor imaging. *Psychiatry Research: Neuroimaging*, *146*(1), 73-82.

Kellner, E., Dhital, B., Kiselev, V. G., & Reisert, M. (2016). Gibbs-ringing artifact removal based on local subvoxel-shifts. *Magn Reson Med*, *76*(5), 1574-1581. https://doi.org/10.1002/mrm.26054

Khundrakpam, B. S., Reid, A., Brauer, J., Carbonell, F., Lewis, J., Ameis, S., Karama, S., Lee, J., Chen, Z., Das, S., Evans, A. C., Brain Development Cooperative, G., Ball, W. S., Byars, A. W., Schapiro, M., Bommer, W., Carr, A., German, A., Dunn, S., Rivkin, M. J., Waber, D., Mulkern, R., Vajapeyam, S., Chiverton, A., Davis, P., Koo, J., Marmor, J., Mrakotsky, C., Robertson, R., McAnulty, G., Brandt, M. E., Fletcher, J. M., Kramer, L. A., Yang, G., McCormack, C., Hebert, K. M., Volero, H., Botteron, K., McKinstry, R. C., Warren, W., Nishino, T., Robert Almli, C., Todd, R., Constantino, J., McCracken, J. T., Levitt, J., Alger, J., O'Neil, J., Toga, A., Asarnow, R., Fadale, D., Heinichen, L., Ireland, C., Wang, D.-J., Moss, E., Zimmerman, R. A., Bintliff, B., Bradford, R., Newman, J., Evans, A. C., Arnaoutelis, R., Bruce Pike, G., Louis Collins, D., Leonard, G., Paus, T., Zijdenbos, A., Das, S., Fonov, V., Fu, L., Harlap, J., Leppert, I., Milovan, D., Vins, D., Zeffiro, T., Van Meter, J., Lange, N., Froimowitz, M. P., Botteron, K., Robert Almli, C., Rainey, C., Henderson, S., Nishino, T., Warren, W., Edwards, J. L., Dubois, D., Smith, K., Singer, T., Wilber, A.

A., Pierpaoli, C., Basser, P. J., Chang, L.-C., Koay, C. G., Walker, L., Freund, L., Rumsey, J., Baskir, L., Stanford, L., Sirocco, K., Gwinn-Hardy, K., Spinella, G., McCracken, J. T., Alger, J. R., Levitt, J., & O'Neill, J. (2013). Developmental Changes in Organization of Structural Brain Networks. *Cerebral Cortex*, *23*(9), 2072-2085. https://doi.org/10.1093/cercor/bhs187

Knudsen, E. I. (2004). Sensitive Periods in the Development of the Brain and Behavior. *Journal of Cognitive Neuroscience*, *16*(8), 1412-1425. https://doi.org/10.1162/0898929042304796

Koenis, M. M., Brouwer, R. M., Swagerman, S. C., van Soelen, I. L., Boomsma, D. I., & Hulshoff Pol, H. E. (2018). Association between structural brain network efficiency and intelligence increases during adolescence. *Human Brain Mapping*, *39*(2), 822-836.

LaMantia, A. S., & Rakic, P. (1990). Axon overproduction and elimination in the corpus callosum of the developing rhesus monkey. *J Neurosci*, *10*(7), 2156-2175. https://www.ncbi.nlm.nih.gov/pubmed/2376772

Lebel, C., & Beaulieu, C. (2011). Longitudinal development of human brain wiring continues from childhood into adulthood. *J Neurosci*, *31*(30), 10937-10947. https://doi.org/10.1523/JNEUROSCI.5302-10.2011

Lebel, C., & Deoni, S. (2018). The development of brain white matter microstructure. *NeuroImage*, *182*, 207-218. https://doi.org/https://doi.org/10.1016/j.neuroimage.2017.12.097

Lenroot, R. K., & Giedd, J. N. (2006). Brain development in children and adolescents: insights from anatomical magnetic resonance imaging. *Neuroscience & Biobehavioral Reviews*, *30*(6), 718-729.

Leppert, I. R., Bontempi, P., Rowley, C. D., Campbell, J. S. W., Nelson, M. C., Schiavi, S., Pike, G. B., Daducci, A., & Tardif, C. L. (2023). Dual-encoded magnetization transfer and diffusion imaging and its application to tract-specific microstructure mapping. *Imaging Neuroscience*, *1*, 1-17. https://doi.org/10.1162/imag_a_00019

Maier-Hein, K. H., Neher, P. F., Houde, J.-C., Côté, M.-A., Garyfallidis, E., Zhong, J., Chamberland, M., Yeh, F.-C., Lin, Y.-C., Ji, Q., Reddick, W. E., Glass, J. O., Chen, D. Q., Feng, Y., Gao, C., Wu, Y., Ma, J., He, R., Li, Q., Westin, C.-F., Deslauriers-Gauthier, S., González, J. O. O., Paquette, M., St-Jean, S., Girard, G., Rheault, F., Sidhu, J., Tax, C. M. W., Guo, F., Mesri, H. Y., Dávid, S., Froeling, M., Heemskerk, A. M., Leemans, A., Boré, A., Pinsard, B., Bedetti, C., Desrosiers, M., Brambati, S., Doyon, J., Sarica, A., Vasta, R., Cerasa, A., Quattrone, A., Yeatman, J., Khan, A. R., Hodges, W., Alexander, S., Romascano, D., Barakovic, M., Auría, A., Esteban, O., Lemkaddem, A., Thiran, J.-P., Cetingul, H. E., Odry, B. L., Mailhe, B., Nadar, M. S., Pizzagalli, F., Prasad, G., Villalon-Reina, J. E., Galvis, J., Thompson, P. M., Requejo, F. D. S., Laguna, P. L., Lacerda, L. M., Barrett, R., Dell'Acqua, F., Catani, M., Petit, L., Caruyer, E., Daducci, A., Dyrby, T. B., Holland-Letz, T., Hilgetag, C. C., Stieltjes, B., & Descoteaux, M. (2017). The challenge of mapping the human connectome based on diffusion tractography. *Nature Communications*, *8*(1), 1349. https://doi.org/10.1038/s41467-017-01285-x

Natu, V. S., Gomez, J., Barnett, M., Jeska, B., Kirilina, E., Jaeger, C., Zhen, Z., Cox, S., Weiner, K. S., Weiskopf, N., & Grill-Spector, K. (2019). Apparent thinning of human visual cortex during childhood is associated with myelination. *Proceedings of the National Academy of Sciences*, *116*(41), 20750-20759. https://doi.org/10.1073/pnas.1904931116

Newman, M. E. (2013). Spectral methods for community detection and graph partitioning. *Physical Review E*, *88*(4), 042822.

Palmer, C. E., Pecheva, D., Iversen, J. R., Hagler, D. J., Sugrue, L., Nedelec, P., Fan, C. C., Thompson, W. K., Jernigan, T. L., & Dale, A. M. (2022). Microstructural development from 9 to 14 years: Evidence from the ABCD Study. *Developmental Cognitive Neuroscience*, *53*, 101044. https://doi.org/https://doi.org/10.1016/j.dcn.2021.101044

Panagiotaki, E., Schneider, T., Siow, B., Hall, M. G., Lythgoe, M. F., & Alexander, D. C. (2012). Compartment models of the diffusion MR signal in brain white matter: a taxonomy and comparison. *NeuroImage*, *59*(3), 2241-2254.

Paus, T. (2010). Growth of white matter in the adolescent brain: myelin or axon? *Brain Cogn*, *72*(1), 26-35. https://doi.org/10.1016/j.bandc.2009.06.002

Rubinov, M., & Sporns, O. (2010). Complex network measures of brain connectivity: uses and interpretations. *NeuroImage*, *52*(3), 1059-1069.

Rudrapatna, U., Parker, G. D., Roberts, J., & Jones, D. K. (2021). A comparative study of gradient nonlinearity correction strategies for processing diffusion data obtained with ultra-strong gradient MRI scanners. *Magn Reson Med*, *85*(2), 1104-1113. https://doi.org/10.1002/mrm.28464

Sairanen, V., Leemans, A., & Tax, C. M. (2018). Fast and accurate Slicewise OutLIer Detection (SOLID) with informed model estimation for diffusion MRI data. *NeuroImage*, *181*, 331-346.

Schaefer, A., Kong, R., Gordon, E. M., Laumann, T. O., Zuo, X.-N., Holmes, A. J., Eickhoff, S. B., & Yeo, B. T. T. (2017). Local-Global Parcellation of the Human Cerebral Cortex from Intrinsic Functional Connectivity MRI. *Cerebral Cortex*, *28*(9), 3095-3114. https://doi.org/10.1093/cercor/bhx179

Schiavi, S., Lu, P.-J., Weigel, M., Lutti, A., Jones, D. K., Kappos, L., Granziera, C., & Daducci, A. (2022). Bundle myelin fraction (BMF) mapping of different white matter connections using microstructure informed tractography. *NeuroImage*, *249*, 118922. https://doi.org/https://doi.org/10.1016/j.neuroimage.2022.118922

Schiavi, S., Ocampo-Pineda, M., Barakovic, M., Petit, L., Descoteaux, M., Thiran, J.-P., & Daducci, A. (2020). A new method for accurate in vivo mapping of human brain connections using microstructural and anatomical information. *Science Advances*, *6*(31), eaba8245. https://doi.org/10.1126/sciadv.aba8245

Schiavi, S., Petracca, M., Battocchio, M., El Mendili, M. M., Paduri, S., Fleysher, L., Inglese, M., & Daducci, A. (2020). Sensory-motor network topology in multiple sclerosis: Structural connectivity analysis accounting for intrinsic density discrepancy. *Human Brain Mapping*, *41*(11), 2951-2963. https://doi.org/https://doi.org/10.1002/hbm.24989

Schilling, K. G., Tax, C. M. W., Rheault, F., Landman, B. A., Anderson, A. W., Descoteaux, M., & Petit, L. (2022). Prevalence of white matter pathways coming into a single white matter voxel orientation: The bottleneck issue in tractography. *Human Brain Mapping*, *43*(4), 1196-1213. https://doi.org/https://doi.org/10.1002/hbm.25697

Seguin, C., Razi, A., & Zalesky, A. (2019). Inferring neural signalling directionality from undirected structural connectomes. *Nature Communications*, *10*(1), 4289.

Seguin, C., Sporns, O., & Zalesky, A. (2023). Brain network communication: concepts, models and applications. *Nature reviews neuroscience*, *24*(9), 557-574. https://doi.org/10.1038/s41583-023-00718-5

Smith, R., Raffelt, D., Tournier, J.-D., & Connelly, A. (2020). Quantitative streamlines tractography: methods and inter-subject normalisation.

Smith, S. M., Jenkinson, M., Woolrich, M. W., Beckmann, C. F., Behrens, T. E., Johansen-Berg, H., Bannister, P. R., De Luca, M., Drobnjak, I., & Flitney, D. E. (2004). Advances in functional and structural MR image analysis and implementation as FSL. *NeuroImage*, *23*, S208-S219.

Suárez, L. E., Markello, R. D., Betzel, R. F., & Misic, B. (2020). Linking structure and function in macroscale brain networks. *Trends in cognitive sciences*, *24*(4), 302-315.

Tamnes, C. K., Roalf, D. R., Goddings, A. L., & Lebel, C. (2018). Diffusion MRI of white matter microstructure development in childhood and adolescence: Methods, challenges and progress. *Dev Cogn Neurosci*, *33*, 161-175. https://doi.org/10.1016/j.dcn.2017.12.002

Tournier, J.-D., Smith, R., Raffelt, D., Tabbara, R., Dhollander, T., Pietsch, M., Christiaens, D., Jeurissen, B., Yeh, C.-H., & Connelly, A. (2019). MRtrix3: A fast, flexible and open software framework for medical image processing and visualisation. *NeuroImage*, *202*, 116137.

Tournier, J. D., Calamante, F., & Connelly, A. (2010). Improved probabilistic streamlines tractography by 2nd order integration over fibre orientation distributions. Proceedings of the international society for magnetic resonance in medicine,

Tustison, N. J., Avants, B. B., Cook, P. A., Zheng, Y., Egan, A., Yushkevich, P. A., & Gee, J. C. (2010). N4ITK: improved N3 bias correction. *IEEE Trans Med Imaging*, *29*(6), 1310-1320. https://doi.org/10.1109/tmi.2010.2046908

Van den Heuvel, M. P., & Sporns, O. (2013). Network hubs in the human brain. *Trends in cognitive sciences*, *17*(12), 683-696.

Veraart, J., Fieremans, E., & Novikov, D. S. (2016). Diffusion MRI noise mapping using random matrix theory. *Magnetic Resonance in Medicine*, *76*(5), 1582-1593.

Vos, S. B., Tax, C. M., Luijten, P. R., Ourselin, S., Leemans, A., & Froeling, M. (2017). The importance of correcting for signal drift in diffusion MRI. *Magnetic Resonance in Medicine*, *77*(1), 285-299.

Wandell, B. A. (1999). COMPUTATIONAL NEUROIMAGING OF HUMAN VISUAL CORTEX. *Annual Review of Neuroscience*, *22*(1), 145-173. https://doi.org/10.1146/annurev.neuro.22.1.145

Ward, I. L., Raven, E. P., de la Rosa, S., Jones, D. K., Teufel, C., & von dem Hagen, E. (2023). White matter microstructure in face and body networks predicts facial expression and body posture perception across development. *Human Brain Mapping*, *44*(6), 2307-2322. https://doi.org/https://doi.org/10.1002/hbm.26211

Yakovlev, P. I., & Lecours, A. R. (1967). *The myelogenetic cycles of regional maturation of the brain*. F. A. Davis Company, Philadelphia, Pa. <Go to ISI>://BIOSIS:PREV19674800116606

Yeh, C. H., Jones, D. K., Liang, X., Descoteaux, M., & Connelly, A. (2021). Mapping structural connectivity using diffusion MRI: Challenges and opportunities. *Journal of Magnetic Resonance Imaging*, *53*(6), 1666-1682.

Yeo, B. T., Krienen, F. M., Sepulcre, J., Sabuncu, M. R., Lashkari, D., Hollinshead, M., Roffman, J. L., Smoller, J. W., Zöllei, L., Polimeni, J. R., Fischl, B., Liu, H., & Buckner, R. L. (2011). The organization of the human cerebral cortex estimated by intrinsic functional connectivity. *J Neurophysiol*, *106*(3), 1125-1165. https://doi.org/10.1152/jn.00338.2011

Zhang, F., Daducci, A., He, Y., Schiavi, S., Seguin, C., Smith, R. E., Yeh, C.-H., Zhao, T., & O'Donnell, L. J. (2022). Quantitative mapping of the brain's structural connectivity using diffusion MRI tractography: A review. *NeuroImage*, *249*, 118870.

8. Supplementary

8.1. Information

A total of 88 children (Mean age = 12.6, SD = 2.9 years, range= 8 - 19 years) were included in the current study (46 female). Figure S1 shows the age distribution of the cohort. The attending parent was asked to complete a brief survey on their demographics and educational attainment. Majority of parents (69/88) had completed a university degree (78%), 11 completed a certificate or diploma (13%) and 8 respondents completed year 12 or less (9%). The Strengths and Difficulties Questionnaire (SDQ) was administered as a measure of emotional/behavioural difficulties (Goodman, 1997). In a subsample of children and adolescents (N=79, 40 males, 39 females), parent-reported total scores (summation of all SDQ modules) were generally low (mean=6.45, SD=3.90, range=0-19) suggesting low levels of internalising and externalising problems in the cohort.

8.2. Figures

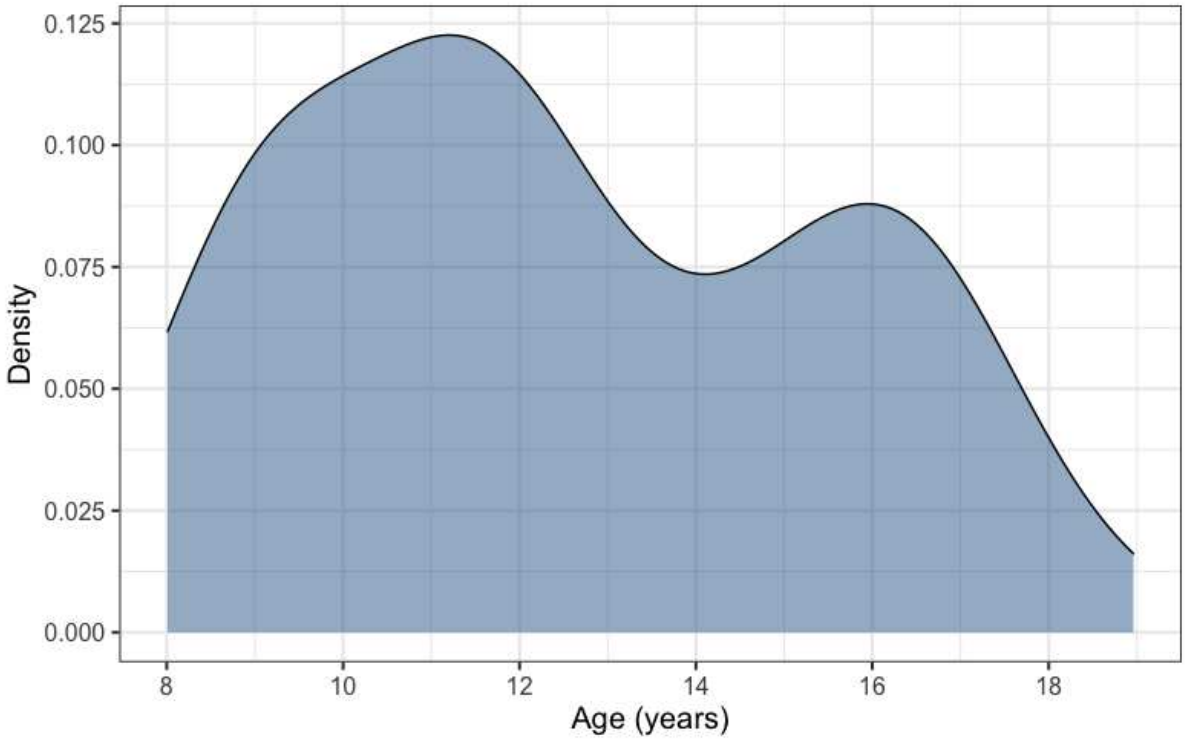

Figure S1: Age distribution of cohort.

Figure S3: Circle plot demonstrating connection strength of canonical networks.

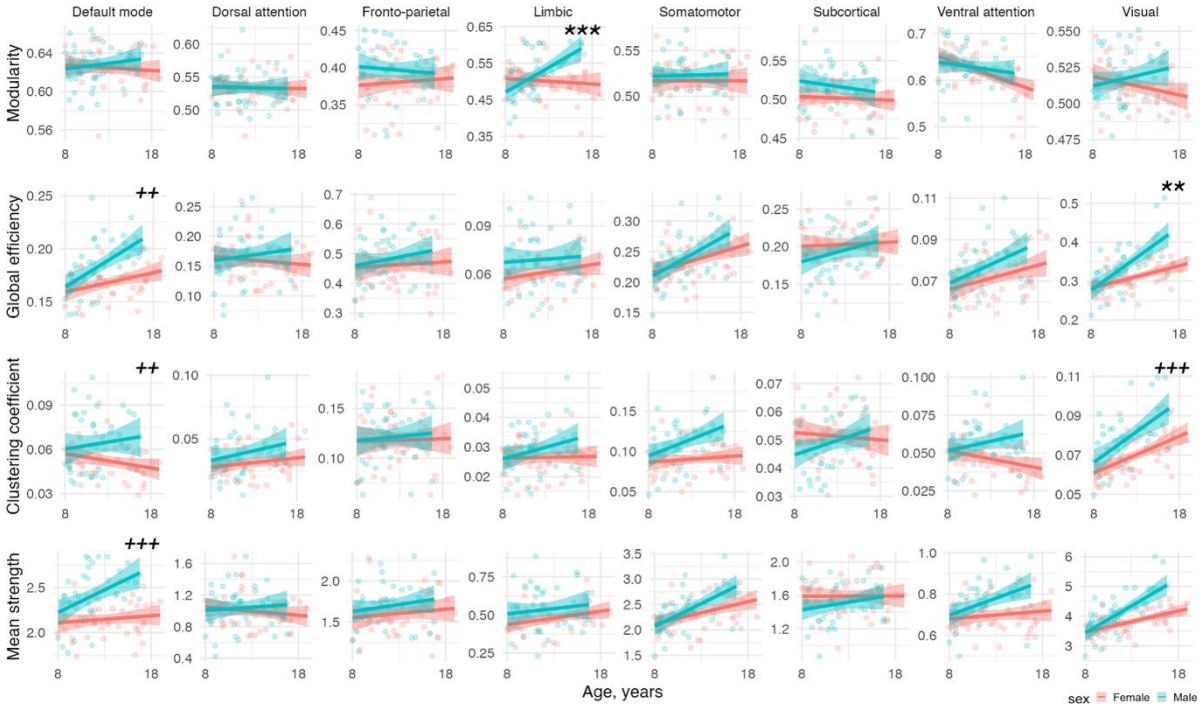

Figure S3: Sex differences in network properties over age. Associations with network measures are annotated in terms of difference in absolute values (main effect: +++=p<.005, ++=p<.01) and in slope over age (interaction term: ***=p<.005, **=p<.01). Red: female, blue: male.

8.3. Tables

Table S1: Voxel-wise diffusivity parameters estimated in a white matter mask for one younger (8-year-old) and one older (17-year-old) participant. Values are reported as mean (SD).

	d_a	d_{par}	d_{perp}
Younger	2.27 (0.71)	2.01 (0.57)	0.61 (0.28)
Older	2.35 (0.62)	1.71 (0.58)	0.62 (0.27)

Table S2: Regions from the Destrieux parcellation assigned to each canonical cortical network. Results for left hemisphere shown (equivalent in right hemisphere). Only nodes overlapping the same network in >80% of participants were included in the analysis.

Region	Name	X	Y	Z	Yeo7_name
2	G_and_S_occipital_inf	23	60	180	visual
3	G_and_S_paracentral	63	100	60	somatomotor
4	G_and_S_subcentral	63	20	220	somatomotor
5	G_and_S_transv_frontopol	13	0	250	dmn
6	G_and_S_cingul-Ant	26	60	0	dmn
7	G_and_S_cingul-Mid-Ant	26	60	75	ventralattention
9	G_cingul-Post-dorsal	25	60	250	dmn
10	G_cingul-Post-ventral	60	25	25	dmn
11	G_cuneus	180	20	20	visual
12	G_front_inf-Opercular	220	20	100	ventralattention
13	G_front_inf-Orbital	140	60	60	dmn
15	G_front_middle	140	100	180	frontoparietal
16	G_front_sup	180	20	140	dmn
17	G_Ins_lg_and_S_cent_ins	23	10	10	ventralattention
18	G_insular_short	225	140	140	ventralattention
19	G_occipital_middle	180	60	180	visual
20	G_occipital_sup	20	220	60	visual
21	G_oc-temp_lat-fusifor	60	20	140	visual
22	G_oc-temp_med-Lingual	220	180	140	visual
23	G_oc-temp_med-Parahip	65	100	20	limbic
24	G_orbital	220	60	20	limbic
25	G_pariet_inf-Angular	20	60	220	dmn
26	G_pariet_inf-Supramar	100	100	60	ventralattention
27	G_parietal_sup	220	180	220	dorsalattention
28	G_postcentral	20	180	140	somatomotor
29	G_precentral	60	140	180	somatomotor

31	G_rectus	20	60	100	limbic
32	G_subcallosal	60	220	20	limbic
33	G_temp_sup-G_T_transv	60	60	220	somatomotor
35	G_temp_sup-Plan_polar	65	220	60	limbic
38	G_temporal_middle	180	60	60	dmn
41	Lat_Fis-post	61	60	100	somatomotor
42	Pole_occipital	140	20	60	visual
43	Pole_temporal	220	180	20	limbic
44	S_calcarine	63	180	180	visual
45	S_central	221	20	10	somatomotor
46	S_cingul-Marginalis	221	20	100	ventralattention
48	S_circular_insula_inf	221	20	220	ventralattention
49	S_circular_insula_sup	61	220	220	ventralattention
50	S_collat_transv_ant	100	200	200	limbic
51	S_collat_transv_post	10	200	200	visual
52	S_front_inf	221	220	20	frontoparietal
56	S_intrapariet_and_P_trans	143	20	220	dorsalattention
57	S_oc_middle_and_Lunatus	101	60	220	visual
58	S_oc_sup_and_transversal	21	20	140	visual
60	S_oc-temp_lat	221	140	20	dorsalattention
61	S_oc-temp_med_and_Lingual	141	100	220	visual
62	S_orbital_lateral	221	100	20	frontoparietal
63	S_orbital_med-olfact	181	200	20	limbic
65	S_parieto_occipital	101	100	180	visual
69	S_precentral-sup-part	21	20	200	dorsalattention
71	S_subparietal	101	60	60	dmn
73	S_temporal_sup	223	220	60	dmn
74	S_temporal_transverse	221	60	60	somatomotor
76	Left-Thalamus-Proper	0	118	14	subcortical
77	Left-Caudate	122	186	220	subcortical
78	Left-Putamen	236	13	176	subcortical
79	Left-Pallidum	12	48	255	subcortical
80	Left-Hippocampus	220	216	20	subcortical
81	Left-Amygdala	103	255	255	subcortical
82	Left-Accumbens-area	255	165	0	subcortical

1107

Table S3: Results of mixed-effect model selection for first level global graph network analysis. Values reported are Akaike Information Criterion (AIC) of each model fit.

Model	Modularity	Global Efficiency	Clustering Coefficient	Mean Strength
M1a	-2816.78	-2549.70	-3792.68	244.49
M2a	-2821.03	-2553.69	-3796.30	237.85
M3a	-2832.02	-2565.74	-3795.91	167.79
M4a	-2860.55	-2575.29	-3814.42	90.46
M1b	-2825.11	-2569.99	-3801.41	215.66
M2b	-2826.42	-2570.17	-3802.19	214.00
M3b	-2840.35	-2586.03	-3804.65	138.97
M4b	**-2865.94***	**-2591.77***	**-3820.31***	**66.60***

Note: Bold indicates lowest AIC for each graph measure; * indicates if the age by network term was significant at p<.005

Footnote: Models tested are as follows:

M1a <- lmer(measure ~ age + sex + network + (1|ID), REML=FALSE, data=data)

M2a <- lmer(measure ~ age * sex + network + (1|ID), REML=FALSE, data=data)

M3a <- lmer(measure ~ age * network + sex + (1|ID), REML=FALSE, data=data)

M4a <- lmer(measure ~ age * sex * network + (1|ID), REML=FALSE, data=data)

M1b <- lmer(measure ~ age + sex + network + ICV + (1|ID), REML=FALSE, data=data)

M2b <- lmer(measure ~ age * sex + network + ICV + (1|ID), REML=FALSE, data=data)

M3b <- lmer(measure ~ age * network + sex + ICV + (1|ID), REML=FALSE, data=data)

M4b <- lmer(measure ~ age * sex * network + ICV + (1|ID), REML=FALSE, data=data)

Table S4: Summary statistics for the relationship between age and global sub-network characteristics, adjusted for connection density.

Network	Modularity		Global efficiency		Clustering coefficient		Mean strength	
	R^2	p-value	R^2	p-value	R^2	p-value	R^2	p-value
Default mode	0.07	0.91	0.37	**0.003**	0.63	0.06	0.43	0.10
Dorsal attention	-0.05	0.82	0.06	0.41	0.16	0.19	0.05	0.24
Fronto-parietal	0.13	0.68	0.12	0.59	0.00	0.95	0.17	0.52
Limbic	0.08	0.09	0.24	0.80	0.20	0.53	0.31	0.87
Somatomotor	0.08	0.70	0.27	**0.001**	0.63	**< .001**	0.33	**< .001**
Subcortical	0.20	0.21	0.03	0.25	0.11	0.74	0.01	0.47
Ventral attention	0.14	**0.002**	0.19	0.02	0.42	0.22	0.23	0.07
Visual	0.19	0.05	0.43	**< .001**	0.57	**< .001**	0.46	**< .001**

Note: Adjusted R^2 determined using a linear model including age, sex, total intracranial volume and connection density. Bold values indicate p<.005.

Table S5: Results from comparison of age-associations of graph measures with reference to the visual network. Bold values indicate networks which have significantly different slopes to the age-relationship in the visual network, generated using linear mixed efforts models.

Network	Global efficiency		Clustering coefficient		Mean strength	
	t	p-value	t	p-value	t	p-value
Visual (reference)						
Default mode	-1.65	.10	-2.91	**.004**	-4.08	**< .001**
Dorsal attention	-2.96	**.003**	-1.17	.24	-5.25	**< .001**
Fronto-parietal	-1.64	.10	-1.66	.10	-3.91	**< .001**
Limbic	-2.04	.04	-1.87	.06	-4.01	**< .001**
Somatomotor	-0.60	.55	-1.16	.25	-1.78	.08
Subcortical	-2.19	.03	-2.19	.03	-4.55	**< .001**
Ventral attention	-1.93	.05	-3.05	**.002**	-4.34	**< .001**
Somatomotor (reference)						
Default mode	-1.05	.29	-1.05	.29	-2.30	.02
Dorsal attention	-2.36	.02	-2.36	.02	-3.48	**< .001**
Fronto-parietal	-1.04	.30	-1.04	.30	-2.13	.03
Limbic	-1.45	.15	-1.45	.15	-2.23	.03
Subcortical	-1.60	.11	-1.60	.11	-2.78	.006

Ventral attention	-1.33	.18	-1.33	.18	-2.56	.011
Visual	0.60	.55	0.60	.55	1.78	.08

Note: model used was the best fitting model deduced from Table S3.

Table S6: Summary statistics for the relationship between age and network statistics computed in parcels obtained from the Desikan Killany atlas for five distinct lobes.

Lobe	Modularity		Global efficiency		Clustering coefficient		Mean strength	
	R^2	p-value	R^2	p-value	R^2	p-value	R^2	p-value
Frontal	0.12	0.82	0.53	**< .001**†	0.52	**< .001**	0.60	**< .001**†
Parietal	0.09	0.02	0.42	**0.002**	0.38	**0.001**	0.45	**< .001**†
Temporal	0.06	0.07	0.33	0.25	0.52	0.90	0.36	0.19
Occipital	0.05	0.21	0.25	**0.002**†	0.15	0.03	0.29	**0.001**†
Subcortical	0.21	0.22	0.03	0.24	0.10	0.76	0.01	0.47

Note: Adjusted R^2 determined using a linear model including age, sex, total intracranial volume and connection density. Bold values indicate p<.005. † indicates statistically significant results without connection density as a covariate in the linear model.

Table S7: Summary statistics for the relationship between age and global sub-network characteristics, adjusted for connection density. Computed using number of streamlines without COMMIT.

Network	Modularity		Global efficiency		Clustering coefficient		Mean strength	
	R^2	p-value	R^2	p-value	R^2	p-value	R^2	p-value
Default mode	.13	.12	-.01	.32	.23	.50	-.03	.42
Dorsal attention	.08	.05	.08	.49	.03	.57	.07	.49
Fronto-parietal	.30	**< .001**	.33	**.002**	.38	**.004**	.42	**< .001**
Limbic	-.01	.15	.19	.34	.11	.56	.19	.52
Somatomotor	.11	.32	.25	**< .001**	.08	.02	.27	**.003**
Subcortical	.27	**< .001**	.02	.77	.06	.34	.02	.61
Ventral attention	.28	.07	.17	.85	.23	.26	.02	.68
Visual	.15	.95	.00	.93	.01	.94	.02	.98

Table S8: Summary statistics for the relationship between age and number of reconstructed streamlines without COMMIT.

Network	Number of streamlines	
	R^2	p-value
Raw whole-brain	**0.22**	**< .001**
Default mode	-0.01	0.49
Dorsal attention	0.01	0.23

Fronto-parietal	**0.19**	**< .001**
Limbic	0.06	0.02
Somatomotor	**0.23**	**< .001**
Subcortical	0.03	0.07
Ventral attention	-0.01	0.50
Visual	-0.01	0.72

1163